Development of an Intelligent Surface Plasmon Resonance Based Sensor: practical examples

Leiva C. Oliveira
Universidade Federal de Rural do Semi-Árido - UFERSA
Mossoró, RN, BR
leiva.casemiro@ufersa.edu.br

José G. O. Saraiva
Universidade Federal de Rural do Semi-Árido - UFERSA
Mossoró, RN, Brazil
jose.saraiva99035@alunos.ufersa.edu.br

Silvio R. F. de Araújo
Universidade Federal de Rural do Semi-Árido - UFERSA
Mossoró, RN, BR
silvio@ufersa.edu.br

Arthur A. de Melo
VIRTUS-CC
Campina Grande, PB, BR
arthur.melo@virtus-cc.ufcg.edu.br

Antonio M.N. Lima
Universidade Federal de Campina Grande - UFCG
Campina Grande, PB, BR
amnlima@dee.ufcg.edu.br

ABSTRACT

Intelligent sensors based on Surface Plasmon Resonance (SPR) require careful integration of the artificial intelligence (AI) capabilities into the operational aspects of measurement, with the development of new tasks, activities, software, processes, or services. This paper presents practical examples of AI interventions for the construction of smart SPR sensors built with the PPBIO prism.

KEYWORDS

surface plasmon resonance, machine learning, intelligent sensor

1 Introduction

The surface plasmon resonance (SPR) based sensor exploits the characteristics of multilayer structures with a metal/dielectric interface to detect biomolecular interactions in real time with high sensitivity. Typically, this multilayer is illuminated under specific conditions of polarization, wavelength, angle, and intensity, causing the excitation of the SPR phenomenon [9]. This optical coupling is very sensitive to any change in this interface (e.g., adsorption of molecules), providing an optical signature for the substance under analysis. The construction and integration of intelligent SPR sensors in a sensing environment require that their fluidics, optical, electronic, and mechanical components operate properly to ensure accurate and reliable measurements.

The use of Machine Learning (ML) in the construction & integration of SPR sensors is an important topic to support improvements in the sensor response, optimization of construction aspects, inclusion of new sensing parameters, new forms of processing, and new possibilities for smart sensing applications [5].

As shown in Figure 1, intelligent interventions can be applied to the design of SPR sensors by investigating configuration, materials and structure to support the phenomenon excitation; in data exploration with easy and inexpensive simulation, data generation for missing data/data augmentation treatment and sensor modeling to predict future scenarios; and embedded in the Digital Processing Unit (DPU) for response processing with the inclusion of intelligent tasks for segmentation, classification and prediction from sensor responses, as well as real-time monitoring of operating conditions. Furthermore, the requirements and standards for intelligent software [3, 6] and intelligent transducers, such as IEEE 1451, must be pursued in terms of quality, reliability, and audit attributes for insertion into industrial environments and application design.

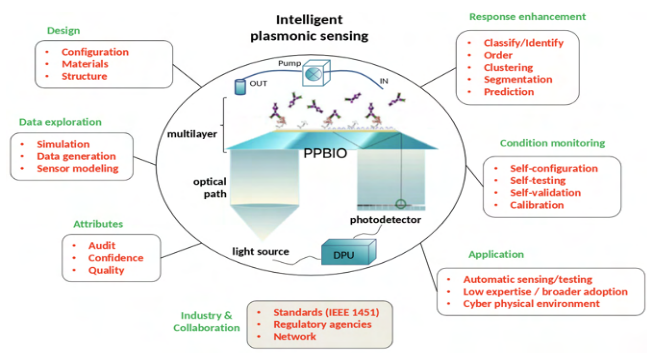

Figure 1: Typical SPR sensor components and examples of intelligent intervention to build intelligent plasmonic sensor.

This work presents practical examples of intelligent intervention development to create smart SPR sensors, with emphasis on SPR sensors based on the PPBIO prism [7]. The PPBIO has a trapezoidal structure, a metalized upper surface to form the metal/dielectric interface, and easy instrumentation with input and output light beams reaching perpendicularly to the multilayer. Details regarding PPBIO SPR sensors are available in [7, 8].

2 Interventions Used in the Intelligent SPR Sensor Conception

The typical responses from an SPR sensor comprise A) the SPR Image, B) the SPR Curve, and C) the Sensorgram, as shown in Figure 2. The image is characterized by a dark shadow indicating the resonance position. The SPR Curve corresponds to a sensitive region (spot) of the image. It is generated to extract the morphological parameters of the curve, such as resonance angle θ_R, minimum value (depth), width (C_R+C_L), and asymmetry (C_R/C_L) [9]. The Sensorgram reflects the temporal evolution of these parameters, indicating the stable instants of the substance and the transitions between them, thus allowing the calculation of kinetic constants[9].

2.1 Image Description

One compact representation of the SPR image benefits the operation and development of smart sensors. As illustrated in Figure 3, a

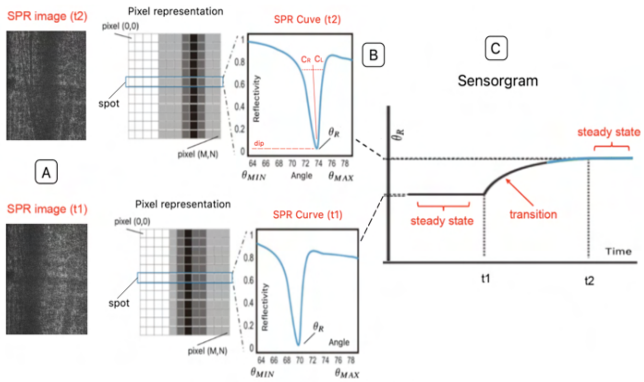

Figure 2: Main SPR sensor data: SPR image, SPR Curve and Sensorgam. Details for pixel representation of the image, the curve characteristics, and the sensorgram's significant moments.

model with an AutoEncoder (AE) network can be used to generate compact latent vectors (z) from SPR images. The influence of the size of z on the quality of the reconstructed image and curve, as well as on the sensor performance, is accompanied by the percentage of image compression as described in [1]. In addition, the generation of latent space forms well-defined clusters that favor the construction of recognition models. Fig. 3b) shows the latent space generated for images with refractive index (RI) 1.33, 1.335, 1.34, 1.345, and 1.35; due to the variation of the resonance position [see images in Fig.3c)].

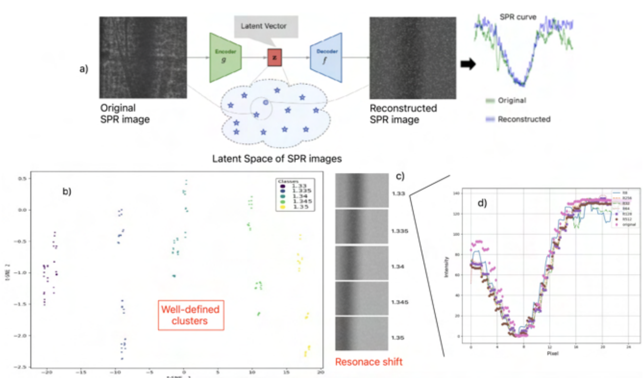

Figure 3: a) AE-model: original SPR image is compacted in the latent vector representation. b) Latent space visualization with T-SNE components. c) Reconstructed image for various RI. d) SPR curves for different sizes of z.

2.2 Substance Recognition

Substance recognition from SPR images using Convolutional Neural Networks (CNN) is an intelligent task that allows the anticipation of the sensor response, minimizes processing steps, saves materials in experiments, accelerates detection, and improves sensitivity. Figure 4 presents a solution based on the MobilNetV2 network trained for substances with RI of 1.33, 1.335, 1.34, 1.345, and 1.35. The results with the deployed model achieved accuracy higher than 96% [see Fig. 4c)] for the identification of the aqueous substances H_2O (RI=1.330), PBS (phosphate buffered saline, RI=1.331) and hypochlorite (hypo, RI=1.345) in the experimental cycle: $H_2O \rightarrow$ HIPO $\rightarrow H_2O \rightarrow$ PBS $\rightarrow H_2O$. For more details about the dataset, model training, and experimental procedures, see [10].

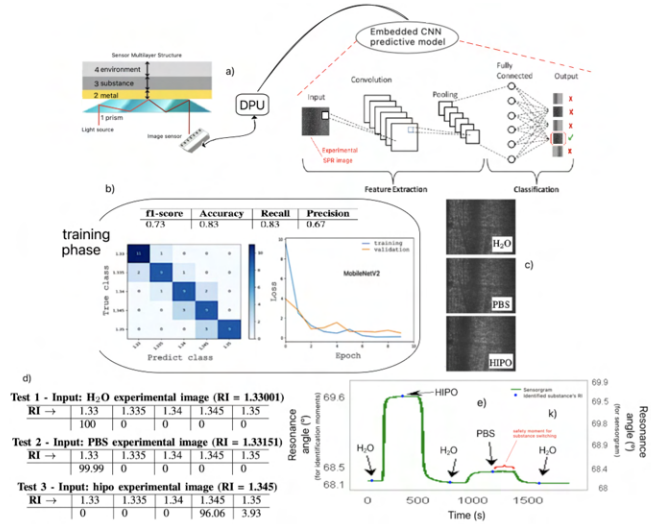

Figure 4: a) SmartSPR sensor with embedded CNN predictive image-based model. b) Evaluation metrics, confusion matrix and loss curve for training phase. c) Experimental SPR images for analyzed solutions. d) Results for the substances recognition with the deployed model. e) Sensorgram recipe, with indication of the recognition moments.

2.3 Image Generation

The recognition process described above can be improved by generating synthetic SPR images using Deep Convolutional Generative Adversarial Networks (DCGAN) [11]. opportunities provided by the model. In the approach illustrated in Figure 6, the generator G and discriminator D networks are trained with SPR images, generating a compact representation (latent vector z) capable of generalizing images for different RI that are visually similar and which present SPR curves with similar characteristics. The simulation of responses to new substances is among the

2.4 Sensorgram Segmentation & Classification

Another practical example is the sensorgram classification. A sensorgram represents the temporal evolution of the sensor response and reflects a well-defined recipe or experimental cycle. Figure 5 illustrates a combined approach of models: linear regression with hypothesis testing (LR & HT) for segmentation and k-Nearest Neighbors (k-NN) for classification. As an example of this combination of models, the sensorgram of the resonance wavelength (λ_R) for the protocol $H_2O \rightarrow Ethanol25\% \rightarrow H_2O \rightarrow Ethanol12.5\% \rightarrow H_2O$ is presented. Details of experimental routes and models execution can be found in [4].

For the LR model, the steady-state regimes are straight lines with slope coefficient β_1 equal to zero, while transitions exhibit $\beta_1 \neq 0$. The regression analysis with β_1 monitoring for a predefined time window has its quality assessed with HT by verifying its value in an acceptable confidence interval (CI). Thus, when hypothesis H_0 for β_1 is zero ($H_0 \Rightarrow \beta_1 = 0$, True), it is confirmed that the data refer to

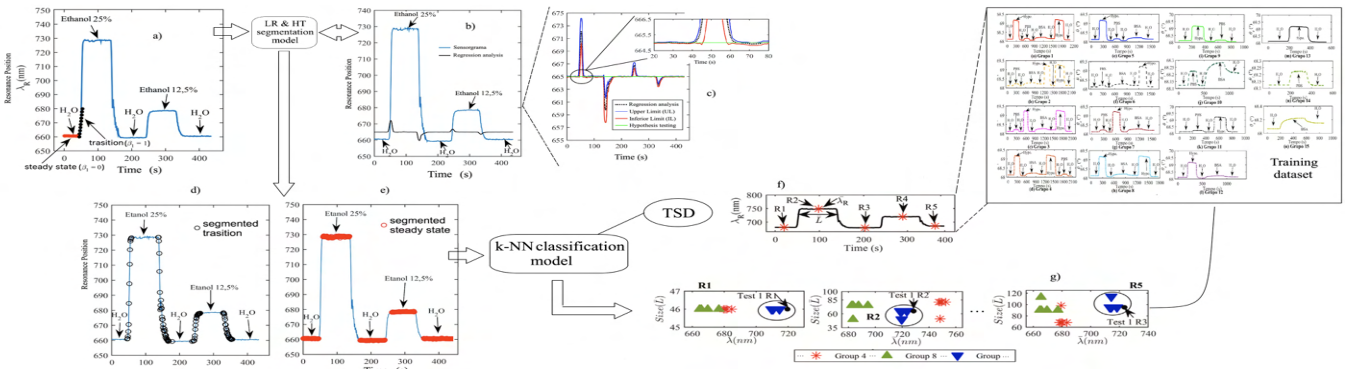

Figure 5: LR & HT model receives a) sensorgram as input and performs b) regression analysis and c) hypothesis testing with predefined CI; highlight that in the interval between 42s to 55s it was not possible to confirm that it is a steady state. Segmented sensorgram into d) transition and e) steady state data. f) The segmented steady state sensorgram is described by the TSD, and g) the k-NN model classifies the sensorgram concerning the amount of permanent regimes and the TSD values of a training dataset.

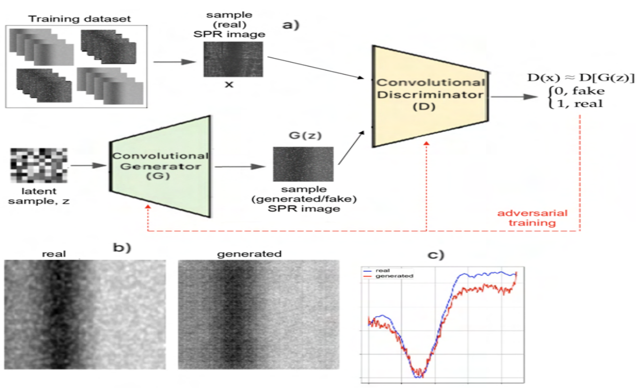

Figure 6: a) DCGAN approach for SPR image generation. b) Examples of real and generated images. c) Respective SPR curves indicating similar features.

a steady-state regime for the confidence level expressed by the CI. Then, the k-NN model is used to classify the Sensorgram with the segmented permanent regimes. Based on the so-called Temporal Sensorgram Descriptor (TSD) [4], the TSD description is used to generate neighbors from the database, and the model calculates the distance for the sensorgram classification.

Automatic Testing

The correct segmentation and classification of sensorgrams allows the inclusion of intelligent tasks for automatic testing. The automatic diagnosis of Dengue fever is illustrated in Figure 7. After the segmentation of the steady states and classification of the sensorgram, a tested sample can be distinguished as *negative test* or *positive test* by checking the error (ϵ_i) of the sample concerning the gold-standard previously saved in memory. The comparison must follow confidence levels governed by regulatory entities and reproducible statistical tests to ensure the quality and auditability of the responses. In the example of Fig. 7b), the CI with the Student's T-test for 99.9% confidence indicates that the current experiment and the gold-standard will be identical if there is an error $\epsilon_i \leq 0.045$ between the sensorgrams. It is worth mentioning that the

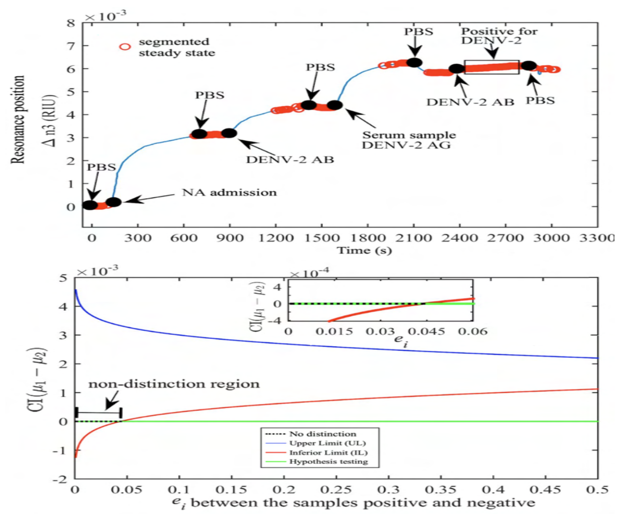

Figure 7: Automatic Dengue diagnosis. a) Sensorgram protocol for DENV-2 SPR detection. b) CI with statistical T-student to confirm positive test.

approach presented to automatically segment, classify, and test SPR Sensorgrams is based on easily explained techniques, favoring the use by regulatory agencies, instead of black box models (e.g. deep learning) considered difficult to interpret and explain.

2.5 Data Filtering

The impact of the SPR curve on the Sensorgram, and consequently on the sensor performance, encouraged the creation of an intelligent filter based on an Artificial Neural Network (ANN) to eliminate the main sources of noise that appear in the SPR curve.

Figure 8 illustrates how the neural network SPR-filter (NNSF) works. The training occurs with the aid of the distortion coefficient matrix (DCM), computed between the experimental and theoretical curves, to select the network architecture to be used: i) single ANN for low DCM values or ii) network committee for high DCM values. The model output is a filtered curve with improved characteristics and attenuated noise, enhancing the sensorgram generation. The results indicate improvements of 68.8% and 77.78% depending on the operating mode and superior metrics concerning the linear model as discussed by [2].

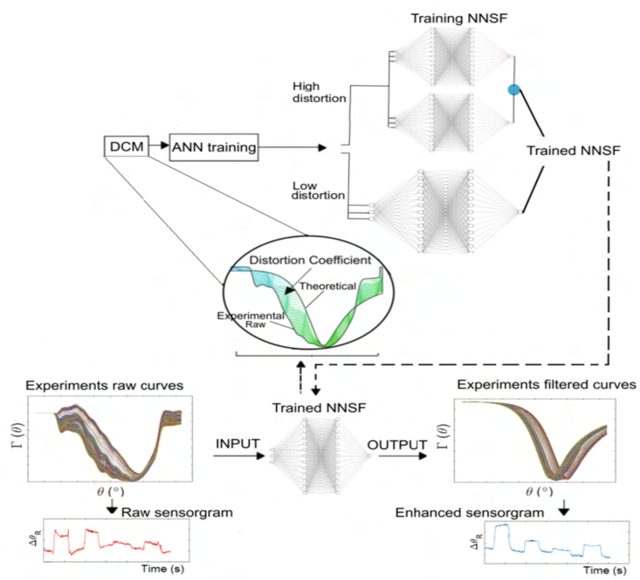

Figure 8: Smart filter principle: distortions between experimental and theoretical curves are used at the training phase and to choose the ANN structure. The trained model is applied to obtain filtered curves, improving the sensorgram responses.

2.6 Automated Calibration

Finally, the intelligent strategy for calibrating the optical elements of the SPR sensor with PPBIO is reported. The diagram in Figure 9 indicates the possible movements of each component. The state machine representation of the self-calibrating algorithm starts with the actual SPR curve depth δ, and ends when $\delta \leq \delta_{\max}$. The one-step move at states ML1, ML2, MP, and MC, can be either forward or backward along the respective movement axis to obtain the best optical coupling.

This automatic calibration procedure avoids manual adjustment of the elements and ensures that the best SPR curve will be obtained. Details of the structure and instrumentation developed to perform the self-calibrating strategy are presented in [12].

3 Conclusion

Artificial intelligence is applied in practical examples, including AI-driven sensor design, data-driven processing, predictive decision-making, data filtering, and mechanical self-calibration. Challenges to providing solutions under industrial, ethical, and regulatory demands & requirements are addressed, leading to opportunities for building AI-powered SPR sensing.

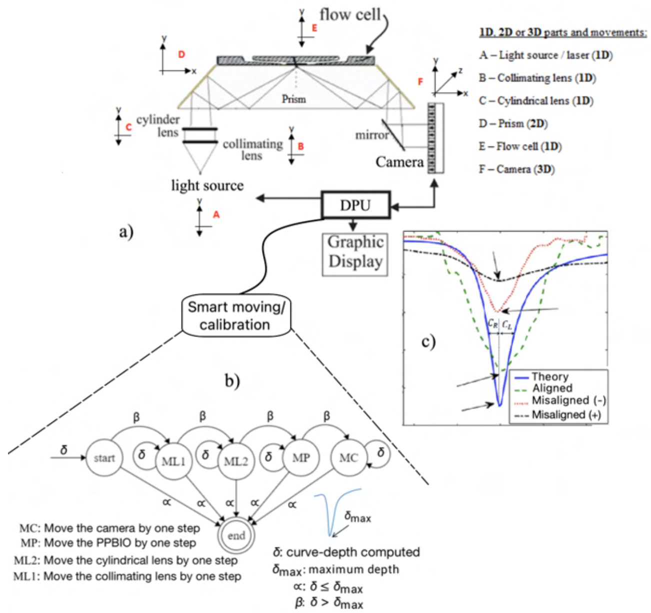

Figure 9: a) Scheme of the PPBIO-based SPR sensor moving parts. b) State machine representation of self-calibrating algorithm. c) SPR curves obtained with the automated platform.

ACKNOWLEDGMENTS

This work has been funded by the project 'SMARTSENS Base System' supported by CENTRO DE COMPETÊNCIA EMBRAPII VIRTUS EM HARDWARE INTELIGENTE PARA INDÚSTRIA - VIRTUS-CC, with financial resources from the PPI HardwareBR of the MCTI grant number 055/2023, signed with EMBRAPII.

REFERENCES

[1] V.G. Barra and et al. 2025. Autoencoder-Based Method for Enhancing and Manipulating Surface Plasmon Resonance Sensor Responses. In *Proceedings of the IEEE LC-IoT 2025*, Vol. 1. IEEE, Fortaleza, 1–5.
[2] J.C.S. Batista and et al. 2020. Smart noise reduction in SPR sensors response using multiple-ANN design. *IEEE Sensors Journal* 21 (2020), 4517–4524.
[3] P.J. Boltryk and et al. 2005. Intelligent sensors - a generic software approach. *Phys.: Conf. Ser.* 15 (2005), 155–160.
[4] J.C. Gomes and et al. 2021. SmartSPR sensor: Machine learning approaches to create intelligent surface plasmon based sensors. *Biosen. & Bioelec.* 172 (2021).
[5] M. Gwiyeong and et al. 2022. Machine learning and its applications for plasmonics in biology. *Cell Reports Physical Science* 3 (2022), 1–16.
[6] A. Meireles and et al. 2021. Towards a Grounded Theory for a Development Process Model for Machine Learning Based Systems. In *Proceedings of the ISE 2021*, Vol. 1. Sociedade Brasileira de Computação, Porto Alegre Brazil, 19–24.
[7] L.C. Oliveira and et al. 2013. A Surface Plasmon Resonance Biochip That Operates Both in the Angular and Wavelength Interrogation Modes. *IEEE TIM* 62 (2013).
[8] L.C. Oliveira and et al. 2016. A Prism-based Polymeric Surface Plasmon Resonance Biochip for Angular and Spectral Modes. *Proc. Engin.* 168 (2016).
[9] L.C. Oliveira and et al. 2019. *Surface Plasmon Resonance Sensors: A Materials Guide to Design, Characterization, Optimization, and Usage* (2 ed.). Springer.
[10] L.C. Oliveira and et al. 2025. Intelligent Surface Plasmon Resonance Sensor For Refractive Index Substance Identification With Convolutional Neural Networks Image-Based Model. *IEEE TIM* 74 (2025), 1–10.
[11] A. Radford and et al. 2016. Unsupervised Representation Learning with Deep Convolutional Generative Adversarial Networks. arXiv:1511.06434
[12] F.J. Silva and el al. 2021. n automated platform for surface plasmon resonance based sensors. *IEEE TIM* 70 (2021), 1–7.